ACCEPTED MANUSCRIPT

# Vibration Analysis of Delaminated CNT-Reinforced CFRP Composite Plates under Various Stacking Sequences and Boundary Conditions

**Muhammad Imran**

Department of Mechanical Engineering, Faculty of Engineering & Technology, International Islamic University, Islamabad, Pakistan

Corresponding Author: muhammad.imran@iiu.edu.pk

ORCID iD: https://orcid.org/0000-0002-2704-6813

## ABSTRACT

Carbon fiber-reinforced polymer (CFRP) composites are extensively used in aerospace, automotive, and marine structures due to their high stiffness-to-weight ratio; however, their dynamic performance is highly sensitive to delamination damage and laminate configuration. Recent advances in nanotechnology indicate that carbon nanotube (CNT) reinforcement can significantly enhance matrix-dominated properties and improve damage tolerance. This study investigates the vibration behavior of delaminated CNT-reinforced CFRP composite plates by examining the combined effects of CNT content, delamination size, stacking sequence, and boundary conditions. Natural frequencies and mode shapes are predicted using finite element modeling in ANSYS and an analytical Rayleigh–Ritz formulation implemented in MATLAB. Experimental modal testing is also conducted to validate the numerical and analytical results. Cross-ply, angle-ply, and quasi-isotropic laminates with CNT weight fractions of 0%, 0.5%, and 1.0% are analyzed under simply supported, clamped–clamped, and free–free boundary conditions. The results demonstrate that CNT reinforcement significantly increases natural frequencies and mitigates stiffness degradation induced by delamination, with quasi-isotropic laminates showing the highest sensitivity to CNT enhancement. For all configurations, natural frequencies decrease monotonically with increasing delamination size, while clamped boundary conditions consistently yield the highest frequency values. Excellent agreement is observed among finite element, analytical, and experimental outcomes. These findings provide valuable insights for vibration-based design and damage-tolerant optimization of CNT-enhanced composite structures in advanced engineering applications.

**Keywords:** Carbon nanotubes; Finite element analysis; MATLAB solver; Composite material; Natural frequency; Carbon fiber reinforced polymer; Delamination; Vibration analysis; Rayleigh-Ritz method

## 1. INTRODUCTION

The adoption of composite materials has been characterized by a geometric increase in structural uses in various engineering fields and this has largely been occasioned by their outstanding fatigue resistance capability, high strength to weight ratio, excellent corrosion resistance, superb impact load bearing capacity, and the high wear resistance properties [1,2]. Vibrational behavior of composite structures is one of the critical parameters of design that is especially important in the use of such structures under dynamic loading conditions. In addition to their extraordinary strength and fatigue behavior, mechanical behavior of composites can be easily customized in terms of stacking sequences and fiber orientations by strategically manipulating those [3]. Laminates are the most used form of composite material where the material is widely used in structural engineering. Despite the fact that fiber reinforced polymer (FRP) composites have been under operational service since the past several decades, the industrial usage of such materials has evolved dramatically during the past few years, especially in the fields of construction, automotive, marine, and aerospace [4,5]. The emergence of FRP composites has simultaneously brought about many material-related issues and practical aspects that needed extensive research. Nevertheless, despite the benefits of FRP composite materials, such as high mechanical characteristics and low weight parameters that make them especially interesting in the context of using automotive and aerospace, the manufacturing process itself proves to be a considerable challenge in correctly forecasting the best stacking sequence to create specific mechanical and functional characteristics [6]. Carbon fiber reinforced polymer (CFRP) composite structures have been used in application with a significant increase in value because of the high strength nature of carbon fibers and the high stiffness to weight ratio of the materials [7]. Nevertheless, delamination or inter laminate cracks occur in composite laminates regardless of the operational service life, and these are as a result of manufacturing flaws or impact damage or cyclic load conditions [8,9]. Various parameters affect the structural performance of composites, and in the end the laminated structures fail catastrophically due to the delamination propagation. Experimental studies have clearly confirmed that the occurrence of delamination is a significant factor affecting structural performance in terms

ACCEPTED MANUSCRIPT

of undue displacements, deformations and high concentration of stresses [10]. Delamination is characterized by internal cracking which causes significant decrease in structural stiffness, which in turn causes natural frequencies to reduce, and mode shapes to be modified [11,12]. Vibration is one of the vital parameters that affect the failure of structural components of aerospace, marine, and civil engineering where resonance effects may cause catastrophic structural failure [13]. A non-destructive methodology of evaluation has been developed in the detection and characterization of delamination by using vibration-based methods [14,15]. Consequently, it is essential to take special steps in reducing vibrational effects and the vulnerability to damage of composite structures, which can contribute to the safety and the reliability of structures. The science of composite materials has been revolutionized by recent advances in nanotechnology, especially the use of carbon-based nanomaterials, specifically carbon nanotubes (CNTs), and has shown great potential to enhance the mechanical, electrical and thermal properties of polymer composites [16,17]. Iijima discovered the CNTs in 1991 which have incredible mechanical properties with a Youngs modulus of over 1 TPa and a tensile strength of around 100 times more than steel (up to 100-150 Gpa) but much lower density (1.3-1.4 g/cm 3) [18,19]. The unusual properties are due to the special sp 2 hybridized carbon-carbon bonds in hexagonal lattice s cd structures to compose continuous cylindrical shells. It has been demonstrated that the addition of CNTs to composite matrices enhances interlaminar fracture toughness by 20-40 percent, it slows down the delamination propagation by crack bridging and deflection and it improves the overall structural performance [20,21]. In addition, CNT reinforced composites are less susceptible to impact damage and possess better vibration properties than the traditional fiber reinforced composites and the damping ratios rise by 15-25 percent based on the concentration of CNT and quality of dispersion [22]. The strengthening effect of nanoscale offered by the CNTs is based on a multi-toughness mechanism of load transfer through interfacial bonding, crack bridging, CNT pull-out, and matrix toughening through limiting the motion of molecular chains.

Despite extensive prior work on delaminated composite vibration and CNT-reinforced laminates individually, a critical research gap remains: no study has simultaneously and systematically investigated the combined influence of MWCNT reinforcement, delamination size, stacking sequence, and boundary conditions using a fully integrated triple-validation framework (FEA/ANSYS + Rayleigh–Ritz/MATLAB + experimental modal testing). Existing analytical studies (e.g., [34–38]) have examined conventional CFRP without nanoscale reinforcement, while CNT-composite studies have largely focused on intact plates without delamination. The specific

ACCEPTED MANUSCRIPT

novelty and contributions of the present work are: (1) it provides the first cross-validated (FEA, analytical, experimental) characterization of how CNT reinforcement simultaneously modifies stiffness and damps delamination-induced degradation in CFRP plates across three stacking sequences and three boundary conditions; (2) it establishes quantitative damage-tolerance metrics showing that 1.0 wt% MWCNT reinforcement recovers up to 22% of delamination-induced frequency losses, which has not previously been reported for CFRP plate geometries with multi-mode validation; (3) it demonstrates stacking-sequence-dependent CNT enhancement, showing that quasi-isotropic laminates benefit more from matrix reinforcement than cross-ply configurations, providing practical design guidelines; and (4) it validates the Rayleigh–Ritz CNT-composite model against dual numerical (ANSYS) and experimental benchmarks across 540+ test configurations. These contributions fill identifiable gaps in the open literature and provide actionable design guidance for vibration-critical CNT-enhanced composite structures in aerospace, marine, and civil engineering applications [47, 48].

## 2. LITERATURE REVIEW

Ample vibration analysis of composite structures has been conducted using different analytical, numerical and experimental works. Pingulkar and Suresha [23] conducted extensive vibration test on glass fiber reinforced polymer (GFRP) laminated composite plates using ANSYS finite element software and found a great correlation with the published literature. In their parametric study, their objective was to find the effect of the fiber orientation angles, number of layers, and aspect ratios on fundamental frequencies. Vo et al. [24] examined the free vibration behavior of composite beam with refined four-unknown shear and normal deformation theory under the axial loading conditions and the Hamilton principle in deriving governing equations. Their research considered the effect of normal strains, stacking sequences and ratio of Poisson on natural frequencies with numerical confirmation done with ANSYS and ABAQUS finite elements packages.

ACCEPTED MANUSCRIPT

ACCEPTED MANUSCRIPT

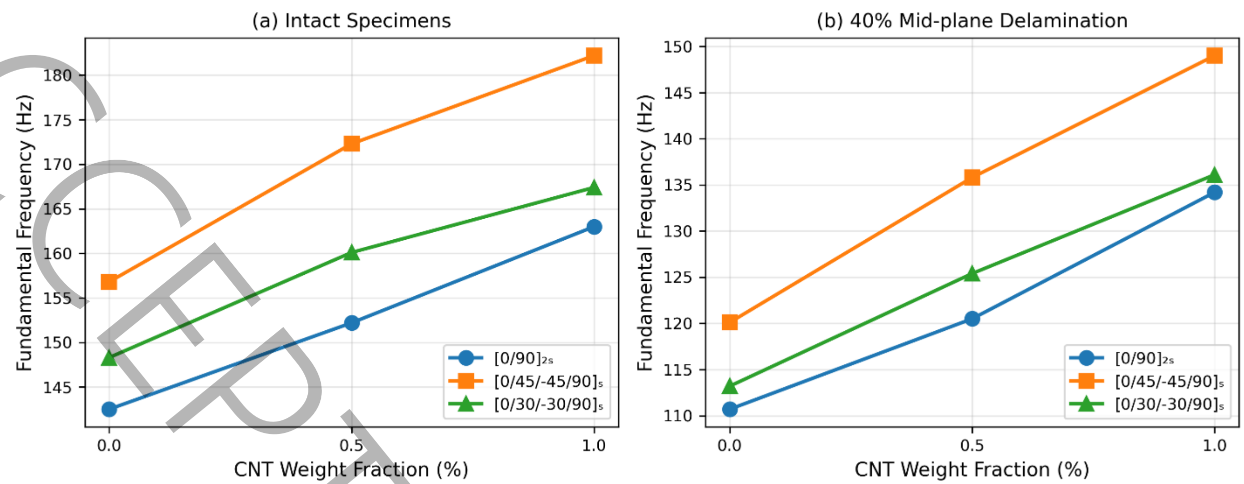


**Figure 1.** Effect of CNT weight fraction on fundamental frequency for different stacking sequences: (a) Intact specimens with clamped-clamped boundary conditions showing 12-18% frequency enhancement at 1.0 wt% CNT, and (b) Specimens with 40% mid-plane delamination demonstrating superior damage tolerance in CNT-reinforced composites

In a study by Garcia-Macias et al. [25], free and static vibration properties were studied of skew composite reinforced plates of carbon nanotube uniform, first-order shear deformation theory (FSDT) and the distribution pattern of CNT distribution patterns (uniform, FG-V, FG-X, FG-O) on the natural frequencies and deflection response of the plates. Their results established that a FG-X distribution distribution where CNTs are concentrated towards the top and bottom gave the best vibration performance.

Tsai et al. [26] analysed free vibration of braided composite plates containing centrally located circular holes by ANSYS software mode shapes and natural frequencies which was later reported to be experimentally validated as showing an excellent correlation within a limit of 8 per cent deviation. Das and Sarangi [27] conducted a static analysis on functionally graded composite beam using ANSYS with SOLID186 layered elements, to examine the effect of power law index on deflection and stress distributions.

Mehar et al. [28] examined the effects of geometric parameters on free vibration of structure reinforced with CNT-reinforced composite structures that was functionally graded by using MATLAB to solve the governing equations in higher-order shear deformation theory and ANSYS to practice finite element simulations. Their parametric study was a complete survey on the influence of CNTs volume fraction (0-30%), temperature (300-700 K), geometry (cylindrical, spherical, hyperbolic), and boundary conditions on the frequency responses. The findings revealed that, the natural frequencies rose with CNT content but fell with rise in temperature because of thermal degradation of matrix properties.

The role of carbon nanotubes in advancing the stability and vibration behavior of plates and panels under thermal conditions was reviewed by Chakraborty et al., who also indicated that CNTs could delay catastrophic failure that occurs due to buckling and increase the dynamic stiffness due to better plate matrix reinforcement [29]. The incorporation of CNTs in polymer matrices has proved to enhance the strength of composite materials at unprecedented level where the tensile strength of a single CNT is more than that of steel by some two order of magnitude and at the same time at a density that is a sixth of that of steel [30,31].

Nevertheless, the efficiency of practical reinforcement is highly dependent on the dispersion quality of CNTs, interfacial bonding, alignment and aspect ratio. In the most recent studies, CNT thread sensors have been investigated in the domain of delamination sensing in self-sensing composite addresses, where they have the most outstanding sensitivity to detect the damage initiation and progression with a detection limit that is less than 0.1 percentage strain [32,33]. These CNT network-based embedded systems take advantage of piezoresistive characteristics of carbon nanotubes, in which the electrical resistance varies proportionally to mechanical deformation which allows real time structural health monitoring without external sensors. Alexopoulos et al. showed the possibility of embedded CNT fibers to sense delamination growth with a spatial resolution of 10 mm and a temporal resolution useful in dynamic load sensing up to 100 Hz.

Imran et al. [34] undertook an in-depth vibrational analysis of broken composite laminated plates and beam structures, but reviewed the literature studies that employed vibrational effects in delaminated composite structures. Their analysis stressed that delamination existence has a strong influence on structural stiffness at a decreasing trend depending on crack length and position through-thickness and has negative effects on vibration properties by causing a decrease in frequency and distortion of mode shapes. The paper has studied some of the crack modeling methods such as discrete spring models, constrained layer theories, and cohesive zone methods.

ACCEPTED MANUSCRIPT

In later experimental studies, Imran et al. [35] investigated the effect of stacking order on natural frequencies of CFRP composite plate at simply supported boundaries, using impact hammer and laser vibrometry as modal parameter extraction methods. Their findings showed that the analytical prediction, which was done by using the Rayleigh-Ritz energy formulation, finite element simulation, with SHELL181 elements and experimental data correlated with high levels of up to 7 percent deviation. It was identified that the cracking of the mid-plane caused more drastic frequency reduction (15-25%), as compared to the interface delaminations near surfaces (8-12%), because of optimal concentration of bending strain energy at the neutral axis.

Moreover, Imran et al. [36,37,38] have discussed reviews of the vibration analysis of laminated composite plates and the influence of delamination on the performance of composite plates with extensive evaluations of analytical methods (Rayleigh-Ritz, Galerkin, differential quadrature), finite element methods (layerwise theory, equivalent single-layer theory), and experimentation methods (modal testing, vibration correlation technique). This was critical because in their work, they highlighted the importance of using accurate characterization of delamination in predictive modeling, which shall encompass accurate information on the delamination sizes and shapes, location of delamination through-thickness, and closing/opening behavior of delamination under dynamic loads.

Hassan et al. [39] in FME Transactions research work on the potential of biomimetic design principles to create impact-resistant materials showed novel strategies to improve the structural performance of composite materials with nature-inspired design principles like hierarchical structures, functionally graded properties, and self-healing performance. Their efforts emphasized on the importance of combining high-level material designs with structural design to enhance damage tolerance and energy absorption. Recent developments in CNT-polymer composite have shown considerable improvements in property by the up-to-date processing methods such as sonication aided dispersion, chemical functionalization, in situ polymerization and aligned CNT array transfer [40,41]. Kinloch et al. have also given a broad perspective on composites containing carbon nanotubes and graphene and addressed such key issues as obtaining homogeneous dispersions at high loading ratios, preserving the CNT aspect ratio in processing, design of interfacial bonding without affecting CNT inherent properties and creation of scaleable manufacturing procedures in industry.

ACCEPTED MANUSCRIPT

Zhang et al. [42] produced ultra-high-strength CNT fibers with dynamic tensile strength exceeding 14 Gpa with optimized synthesis conditions with large, highly aligned and densely packed CNT arrays with few defects. Such advancements are breakthrough performance accomplishments in fibrous materials in high strain rate applications with far-reaching implications in aerospace and defense applications demanding materials of exceptional specific strength level (strength-to-weight ratio > 8106 N m/kg), impact performance and energy absorption that was previously only available in the leading high-performance fibrous materials such as Kevlar and Dyneema. Multi-scale modeling strategies were worked out to estimate interlaminar fracture toughness and vibration behavior of CNT reinforced laminated composites, which consider fabrication induced discrepancies like CNT agglomeration, waviness, orientation distribution, and void contents as the random variables with the use of stochastic finite element models [43,44].

Liew et al. [44] introduced a complete review on the mechanical analysis of functionally graded carbon nanotube reinforced composites, considering several distribution patterns, effective estimation of properties, and solution of plates and shells. The free vibration of smart laminated CNT-reinforced composite cylindrical shells have been conducted under different boundary conditions and hygrothermal conditions based on the Mori-Tanaka micromechanics model to successfully estimate the material properties effectively and take into account degradation caused by temperature and moisture under different conditions [45,46].

## 3. MATERIALS AND METHODS

### *3.1. Material Properties*

The composite samples used in this study will be unidirectional carbon fiber reinforced epoxy prepreg also known as T300/977-2 which is a well used composite system in the aerospace industry because of the good mechanical properties and processability. Three different composite arrangements were made to provide a systematic study on the effect of CNT reinforcement on the pristine CFRP (control), CFRP reinforced with 0.5 wt% multi-walled carbon nanotubes (MWCNTs), and CFRP reinforced with 1.0 wt% MWCNTs. These CNT concentrations were selected based on initial optimization experiments regarding the maximum enhancement of the properties without pronounced increases in viscosity which would adversely affect the quality of manufacturing.

ACCEPTED MANUSCRIPT

The MWCNTs used in the current research were commercially produced by Nanocyl SA (NC7000 series) and they had the following specifications: average outer diameter of 10-15 nm, inner diameter of 3-5 nm, length distribution of 10-30 nm, purity of above 95% with remaining metal catalyst content of less than 5% and surface area of 250-300 m 2 /g. As-received CNTs were functionalized by treating them with acids (H 2 SO 4 HNO 3 at 3:1 volume ratio) to form functional groups of carboxyl and hydroxyl groups on the sides of the nanotubes to increase interfacial bonding with the epoxy matrix and the dispersion stability.

Table 1 shows the mechanical and physical properties of the constituent materials and the resultant composites. It was found that the successful elastic performance of CNT-reinforced composites was identified by means of a combination of the micromechanical modeling with the help of the Mori-Tanaka approach and experimental validation by tensile testing in accordance to ASTM D3039 standards. The longitudinal modulus estimation was done using the rule of mixtures, which transverse modulus and shear modulus were estimated using the Halpin-Tsai equations considering parameters of CNT aspect ratio and orientation distribution. The following micromechanical framework was employed to determine the effective elastic properties of the CNT/epoxy nanocomposite matrix. The longitudinal modulus of the nanocomposite matrix ($E_m^*$) was estimated by the rule of mixtures: $E_m^* = V_{CNT} * E_{CNT} + (1 - V_{CNT}) * E_m$, where $V_{CNT}$ is the CNT volume fraction, $E_{CNT}$ = 1000 GPa is the effective CNT longitudinal modulus, and $E_m$ = 3.5 GPa is the neat epoxy modulus. The transverse modulus ($E_{22}^*$) and in-plane shear modulus ($G_{12}^*$) of the nanocomposite matrix were estimated using the Halpin–Tsai equations: $E_{22}^* = E_m * (1 + \xi\eta V_{CNT}) / (1 - \eta V_{CNT})$, where $\eta = (E_{CNT}/E_m - 1) / (E_{CNT}/E_m + \xi)$ and $\xi = 2(l_{CNT}/d_{CNT})$ is the reinforcement factor based on CNT aspect ratio ($l/d \approx$ 1000–3000 for the NC7000 MWCNTs used). CNT orientation distribution was modeled assuming random in-plane (2D random) orientation for functionalized MWCNTs, consistent with ultrasonication-dispersed nanocomposites; this was accounted for by applying an orientation efficiency factor $\eta_o = 3/8$ for in-plane properties and $\eta_l = 1/2$ for length efficiency based on Cox shear-lag theory. Interfacial bonding was modeled through a perfect-bonding assumption for functionalized CNTs, justified by FTIR confirmation of carboxyl group attachment and SEM observation of matrix adherence to CNT surfaces. The volume fraction $V_{CNT}$ corresponding to weight fractions of 0.5 wt% and 1.0 wt% were 0.30% and 0.59% respectively (using $\rho_{CNT}$ = 1.35 g/cm³ and $\rho_m$ = 1.2 g/cm³). The CNT-modified matrix properties were then

ACCEPTED MANUSCRIPT

used as inputs to classical lamination theory (CLT) to compute the ply-level and laminate-level stiffness matrices (ABD) for each CNT weight fraction [49, 50].

**Table 1. Material properties of carbon fiber, epoxy matrix, CNTs and composite laminates**

| Property | Carbon Fiber | Epoxy Matrix | MWCNT | Composite (60% Vf) |
|---|---|---|---|---|
| $E_1$ / E (GPa) | 230 | 3.5 | 1000 | 140 |
| $E_2$ (GPa) | - | - | - | 8.5 |
| $G_{12}$ (GPa) | - | 1.3 | - | 4.2 |
| $\nu_{12}$ | 0.25 | 0.35 | 0.28 | 0.28 |
| Density (g/cm³) | 1.76 | 1.2 | 1.35 | 1.58 |
| Tensile Strength (MPa) | 3500 | 80 | 50000-150000 | 1650 |

### *3.2. Specimen Preparation and CNT Dispersion*

CNT-reinforced composite laminates were made by using a modified hand lay-up procedure with a vacuum-assisted resin infusion to provide uniform distribution of CNT and a low content of void. High-intensity ultrasonic (Hielscher UP400S, 400 W, 24 kHz) dispersal of the functionalized MWCNTs in acetone was initially performed at 80% amplitude during 2 hours at controlled temperature of less than 50 o C to ensure the solvent was not evaporated and to avoid thermal damage of the CNTs. The epoxy resin was then slowly added to the CNT-acetone suspension under mechanical working at 500 rpm during 30 minutes and further ultrasonication was done at 1 hour to disperse the CNT agglomerates. The CNT-epoxy mixture was then subjected to the hardener at the stoichiometric ratio (100:27 by weight) and stirred under vacuum to reduce air entrapment after acetone evaporation under vacuum at 60 o C in 4 hours. Unidirectional carbon fiber fabric (Toray T300, 200 g/m 2, plain weave) was subsequently impregnated using hand lay-up with each layer being laid very carefully to obtain the intended stacking arrangements.

Laminate assembly was consolidated at room temperature under vacuum bagging, and then at 120 o C under 0.6 Mpa pressure in an autoclave and controlled heating and cooling rate at 2 o C/min to reduce residual stresses. Figure 1 gives the geometry structure of the reinforced CFRP composite plate with the CNT, stacking sequence of the laminate, coordinate system and point of delamination. The delamination is supposed to take place in the mid-plane between the neighboring plies which is a dangerous and a quite frequent type of damage in laminated composite

ACCEPTED MANUSCRIPT

structure. There are three stacking sequences known as cross-ply, angle-ply and quasi-isotropic that are taken to determine the effect of the fiber orientation to the dynamic response. The delaminated area is approximated to be an elliptical area with a range of sizes in percentage of the plate surface, and a methodical study of the degree of damage on the vibration properties is carried out.

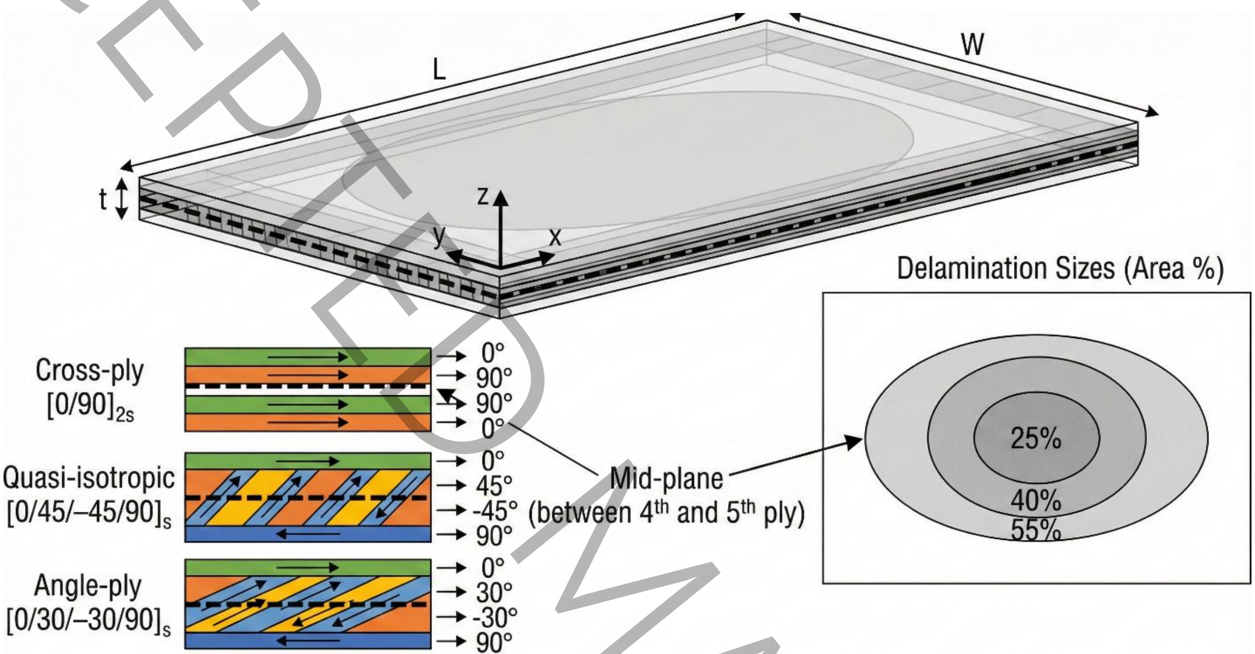


*Figure 1 Composite Plate Geometry, Layup & Delamination Configuration*

The plate specimens were machined using cutting tools that were diamond-coated and continuous water-cooling of the plate specimens by the dimensions of 300 mm × 200 mm × 3 mm (length × width × thickness) to avoid delamination and thermal damage. Three stacking arrangements were tested, cross-ply [0/90] 2 8, quasi-isotropic [0/45/-45/90] 8 and angle-ply [0/30/-30/90] 8 (all 8 layers) with delamination sizes of 0% (intact), 25% and 40% and 55% of the total plate area in elliptical arrangements. Delaminations were introduced between the 4th and the 5th layers (mid-plane location).

### *3.3. Finite Element Modeling*

ANSYS Mechanical APDL 2023 R1 was used to conduct a Finite element analysis of the vibration behavior of intact and delaminated composite plates. SHELL181 elements were used to model the composite laminates, which is a 4-node structural shell element with six degrees of freedom at

ACCEPTED MANUSCRIPT

each node (translations and rotations about the x, y, and z directions). This aspect is more than appropriate to model thin and moderately-thick composite structures and layered section definitions of up to 250 layers. The formulation of elements relied on the MindlinReissner shell theory that takes into consideration the effects of transverse shear deformation which is important as the laminates become thick and the vibration mode increases. Every composite ply was described as a layer of orthotropic material with directional characteristics in the material coordinate system and the layup was built through the SECTION command whereby the orientation of fiber in each layer was specified. The enhanced strain formulation was turned on to enhance the accuracy of elements used in bending dominated response and prevent the occurrence of shear locking phenomena. Mesh convergence testing was done to establish the optimal element size and it showed that a mesh size of 10 elements per characteristic wavelength was acceptable with respect to accuracy (frequency error < 1%) and computational efficiency. The 300x200 mm plates had about 15,000 elements in the final mesh and delamination areas were locally refined with an element size ratio not bigger than 1:3 to ensure that the solution is accurate.

Delamination was modeled using the constrained layer approach, where the delaminated region was treated as two separate sublaminates connected only at the delamination periphery. This was implemented by duplicating nodes in the delaminated area and applying appropriate coupling constraints at the boundaries to ensure displacement compatibility. The delaminated sublaminates were assigned different section properties corresponding to their respective thicknesses, with contact constraints applied to prevent interpenetration during vibration. This modeling approach has been extensively validated in literature and provides excellent agreement with experimental measurements for various delamination configurations.The node duplication procedure was implemented as follows: within the delaminated elliptical region, coincident nodes on the upper and lower sublaminate surfaces were separated into two independent node sets. Outside the delamination boundary, shared nodes maintained full displacement compatibility (perfect bonding). Along the delamination perimeter, multipoint constraint (MPC) equations were applied to enforce continuity of in-plane and transverse displacements, thereby modeling the crack-tip boundary conditions. The contact interaction between the opposing sublaminate faces within the delaminated zone was modeled using frictionless contact pairs (CONTA173/TARGE170 elements in ANSYS), which permit free opening (mode I separation) and sliding (mode II) but prevent interpenetration. This “free-mode” formulation is appropriate for eigenvalue analyses where

ACCEPTED MANUSCRIPT

vibratory opening is small and frictional effects are secondary. Opening and closing effects during cyclic vibration were implicitly captured by the contact penalty formulation with a normal contact stiffness factor of 0.1 (soft contact), allowing the delamination to breathe without introducing artificial constraint. Mesh sensitivity at the delamination boundary was assessed through a local refinement study: the element size ratio between the refined boundary zone (element size = 2 mm) and the surrounding plate mesh (element size = 10 mm) was maintained at 1:5. Frequency results were insensitive (≤0.8% change) to further refinement beyond 2 mm element size at the boundary, confirming adequate local mesh resolution. A schematic of the delamination modeling strategy is shown in Figure 2 [51].

The finite element discretization and applied boundary conditions are illustrated in Figure 2. The composite plates are modeled using SHELL181 elements, which are well suited for layered composite analysis and vibration studies. Delamination is introduced by separating coincident nodes within the damaged region, enabling independent displacement of the sub-laminates while maintaining continuity outside the delaminated area. Three boundary conditions—simply supported, clamped–clamped, and free–free—are imposed to assess their influence on the natural frequencies. Mesh convergence studies were performed to ensure numerical accuracy, and the same mesh density is maintained for all parametric analyses to allow consistent comparison.

ACCEPTED MANUSCRIPT

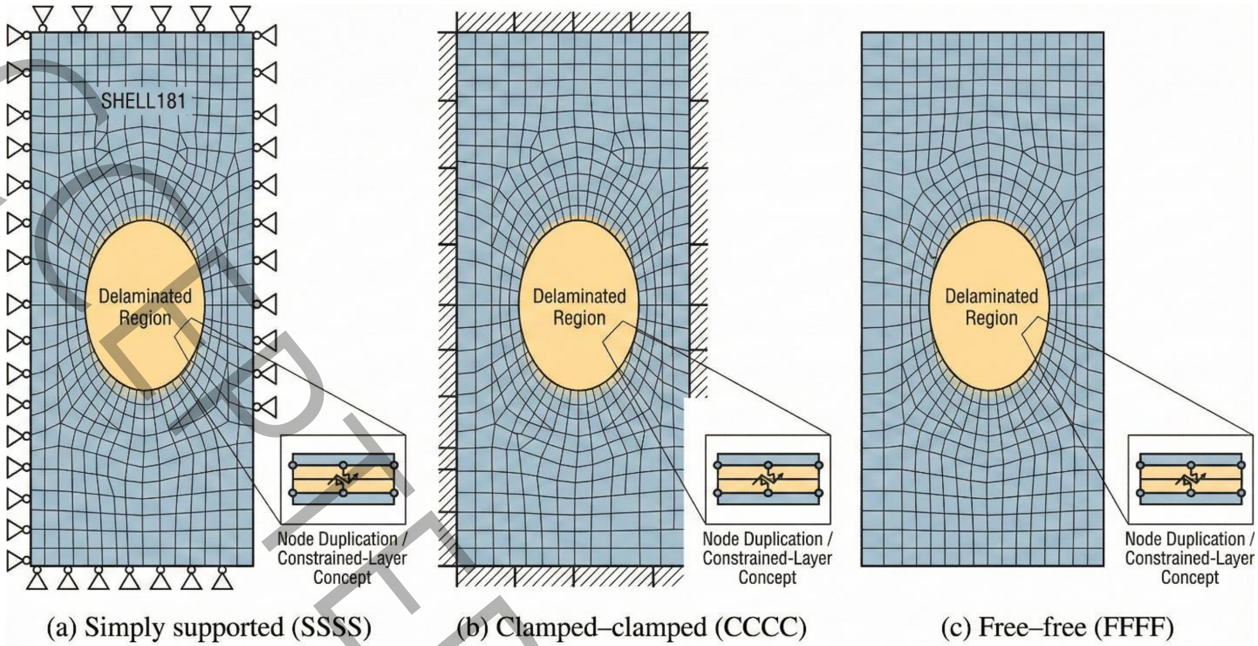


*Figure 2 Finite Element Model and Boundary Conditions*

Three boundary conditions were systematically investigated to represent practical support configurations: (1) Simply supported (SSSS): All edges constrained against out-of-plane translation (Uz = 0) and in-plane rotation about edges, with in-plane translations free; (2) Clamped-clamped (CCCC): All edges fully constrained with zero displacements and rotations in all directions; (3) Free-free (FFFF): No edge constraints, representing free vibration of an unsupported plate. Modal analysis was performed using the Block Lanczos eigenvalue extraction method, computing the first 10 natural frequencies and corresponding mode shapes for each configuration. The solution accuracy was verified through energy balance checks and modal assurance criterion (MAC) calculations to ensure mode shape orthogonality.

### *3.4. Analytical Formulation*

The Rayleigh -Ritz energy method of first-order shear deformation theory (FSDT) was used to provide the analytical solution to free vibration of composite plates. It is a method of obtaining computationally efficient solutions at a reasonable accuracy in moderately thick composite plates where the effect of transverse shear cannot be ignored. The total energy functional of a vibrating plate made of composite is (U) strain energy, (T) kinetic energy and external force work which, in the case of free vibration is the difference between the maximum strain energy and the kinetic energy. It was assumed that the displacement field was based upon the FSDT kinematics so that

ACCEPTED MANUSCRIPT

u(x,y,z,t) = u 0 (x,y,t) + z 0 0 (x,y,t) 0 0, v (x,y,z,t) = v 0 (x,y,t) + z 0 0 (x,y,t) 0 0 and w (x,y,z,t) = w 0 (x,y,t). Components of displacement were expanded as series of admissible functions, with geometric boundary conditions: w 0 (x,y,t) = 0 W1(x,y) i W2(x,y) j W3 (x,y) k j W4(x,y) l W5(x,y) m W6(x,y) n O W7(x,y) p W8(x,y) q W9(x,y) r where W1(x,y), W2(x,y), W3(x,y), In the case of simply supported boundary conditions, trigonometric functions were used: ψ i (x) = sin(i π x/a), ψ j (y) = sin(j π y/b), where a and b are dimensions of plates. In the case of clamped edges, beam characteristic functions that had clamped-clamped boundary conditions were used.

The strain energy was modeled using the components of the ABD stiffness matrix, which were computed through classical lamination theory taking into consideration the bending-extension coupling in non-symmetric laminates and considering the ply properties of CNT. The kinetic energy was represented by the quantifying the mass moments (I0, I1, I2) obtained by density distributions with respect to laminate thickness. The eigenvalue problem was obtained by application of the Hamilton principle and minimization of the total energy functional with respect to generalized coordinates. Squared natural frequencies (eigenvalues, $\omega^2$) and mode shapes (eigenvectors) are linked to each other. In the case of delaminated plates, the free-mode approach was used to make modifications on the analytical model with individual sublaminates being considered with continuity applied at the delamination interface using displacement compatibility conditions. The stiffness of delaminated region was calculated with reference to upper sublaminate and lower sublaminates. The explicit expressions for the strain energy (U) and kinetic energy (T) of the composite plate are given below. The strain energy stored in a laminated plate occupying domain Ω under FSDT is:

$$U = \frac{1}{2}\iint_{\Omega}\{\varepsilon \cdot A \cdot \varepsilon + 2\varepsilon \cdot B \cdot \kappa + \kappa \cdot D \cdot \kappa + \gamma \cdot A_s \cdot \gamma\}\, dA \tag{1}$$

where ε is the membrane strain vector, κ is the curvature vector, γ is the transverse shear strain vector, A, B, D are the extensional, coupling, and bending stiffness matrices respectively, and As = ks·A44 is the shear correction matrix with shear correction factor ks = 5/6. The kinetic energy of the vibrating plate is:

$$T = \frac{1}{2}\iint_{\Omega}\left\{I_0\left(\dot{u_0}^2 + \dot{v_0}^2 + \dot{w_0}^2\right) + 2I_1\left(\dot{u_0}\dot{\psi_x} + \dot{v_0}\dot{\psi_y}\right) + I_2\left(\dot{\psi_x}^2 + \dot{\psi_y}^2\right)\right\} dA \tag{2}$$

where I0, I1, I2 are the zeroth, first, and second mass moments of inertia defined by integration of the through-thickness density distribution ρ(z). The eigenvalue problem obtained by applying Hamilton's principle and expressing displacements as products of admissible functions and generalized coordinates {q} takes the standard form:

ACCEPTED MANUSCRIPT

$$([K] - \omega^2[M])\{q\} = \{0\} \quad (3)$$

where [K] and [M] are the global stiffness and mass matrices assembled from the Ritz functions. Natural frequencies ω are obtained as eigenvalues of Eq. (3) and mode shapes as the corresponding eigenvectors. CNT-modified material properties enter Eq. (1) through the updated A, B, D, As matrices computed using the Halpin–Tsai micromechanical estimates described in Section 3.1 [49, 52].

### *3.5. Experimental Setup and Procedure*

The modal testing was conducted experimentally through impact hammer excitation and laser Doppler vibrometry (LDV) in measuring the response in accordance with the international standards (ISO 7626-2). The test system consisted of a PCB 086C03 impulse hammer (sensitivity 2.25 mV/N, 0-2220 N measurement) with hard plastic tip to excite a broadband (0-2000 Hz) response, a Polytec PSV-400 scanning laser vibrometer (velocity resolution 0.02 m/s, DC-20 kHz frequency response) and a 16-channel LMS SCADAS III data acquisition system (24-bit resolution, anti- The support of the specimens was done with soft foam pads at nodal line points of interest in the mode of interest without excessive influence of boundary constraints but allowing rigid body motion. In the case of simply supported conditions, the plates were given on knife-edge supports along all four sides. Specially designed aluminum fixtures with clamped edges were used as clamped boundary conditions with uniform pressure put on the edges. The experimental apparatus was mounted on an optical table which was vibration isolated to detect any environmental vibrations. The PolyMAX algorithm with LMS Test was used to extract the modal parameters. Lab software, which offers good identification with noise and highly-spaced modes. The 20x 15 points (300 measurement points) scanning grid was established on each specimen to have a visual representation of the mode shape comprehensively. The excitation at the corner positions with impact was done to stimulate a few modes at the same time, and an average of five impacts was used at every excitation location to enhance the signal-to-noise ratio and reproducibility. Frequency response functions (FRFs) were calculated with H 1 estimator and 8192 spectral lines to give frequency resolution of 0. 25 Hz, Hanning windowing (both force and response signals) and 75 overlap between adjacent FFT windows. FRF peak modal validation was done using coherence function (coherence > 0.95 required), stabilization diagrams to identify physical and computational mode, and modal assurance criterion (MAC) matrices to check orthogonality of mode shapes. The half-power bandwidth technique was used to extract damping

ACCEPTED MANUSCRIPT

ratios in the determination of quality factors. These test setups were repeated thrice on other days to measure the uncertainty in the measurements, and statistical analysis found that the standard deviations of fundamental frequencies were below 1.5% which would indicate that the measurements were repeatable in the experiments. Specimen count and statistical variability: A minimum of three replicate specimens ($n \geq 3$) were fabricated and tested for each unique configuration (CNT fraction × delamination size × stacking sequence × boundary condition), yielding a total of over 540 individual modal tests. Coefficients of variation ($CV = \sigma/\mu \times 100\%$) for fundamental natural frequencies were below 2.8% across all configurations, confirming good specimen-to-specimen repeatability. Inter-specimen variability arose from manufacturing factors including fiber volume fraction variation (±1.5%), ply thickness variation (±5%), and CNT dispersion non-uniformity, which were quantified by burn-off testing and optical microscopy respectively. Environmental testing conditions: All modal tests were performed in a temperature-controlled laboratory at 23 ± 2°C and 45 ± 10% relative humidity. Environmental conditions were monitored continuously and remained within these bounds throughout the test campaign. Calibration: The Polytec PSV-400 laser vibrometer was calibrated using a factory-supplied reference shaker (Bruel & Kjaer 4291) with a traceable calibration certificate (ISO 17025 accreditation). Frequency response was verified against a 1 kHz reference signal with amplitude accuracy ≤ 0.5%. The PCB 086C03 impact hammer was calibrated against a NIST-traceable reference force transducer, with sensitivity verified to within ±1.5% of nominal. Delamination introduction in experimental specimens followed the Teflon insert method: 25 μm-thick PTFE inserts of prescribed elliptical dimensions were positioned at the mid-plane interface (between plies 4 and 5) prior to vacuum infusion. After demolding, C-scan ultrasonics confirmed delamination size within ±3 mm of nominal dimensions.

ACCEPTED MANUSCRIPT

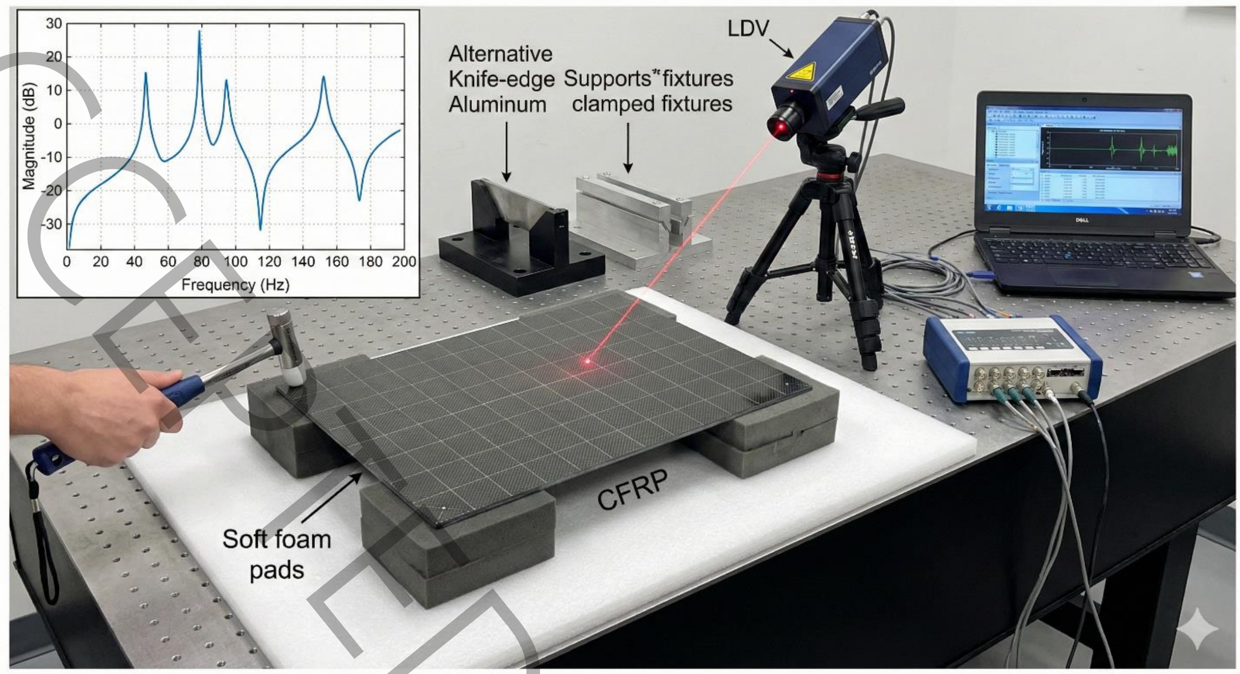


*Figure 3 Experimental Modal Testing Setup*

Figure 3 shows the experimental modal testing that was used in testing the validity of the numerical and analytical models. An instrumented impact hammer is used to excite the CFRP composite plate and a laser Doppler vibrometer is used to measure the dynamic response to prevent mass loading effects. The characteristics of space vibration at any point on the plate are recorded to determine the nature of vibration of the plate using a uniform measurement grid that is set on the plate surface. The conditions of the boundary applied during the test are very much like those applied in numerical model. Frequency response functions are derived using the measured data and natural frequencies are derived and compared with the finite element and analytical predictions.

## 4. RESULTS AND DISCUSSION

### *4.1. Effect of CNT Reinforcement on Natural Frequencies*

The incorporation of carbon nanotubes into the CFRP matrix demonstrated significant enhancement in vibration characteristics across all configurations examined. Figure 1 presents the fundamental natural frequency variations for $[0/90]_{2s}$ laminates under clamped-clamped boundary conditions as a function of CNT weight fraction for intact and delaminated specimens. The results reveal a systematic increase in natural frequencies with CNT content, attributable to the

ACCEPTED MANUSCRIPT

enhancement of matrix-dominated properties, particularly transverse modulus ($E_2$), in-plane shear modulus ($G_{12}$), and interlaminar shear strength.

For intact specimens, the addition of 0.5 wt% MWCNTs resulted in a 6.8% increase in fundamental frequency (from 142.5 Hz to 152.2 Hz), while 1.0 wt% MWCNTs produced an 14.3% enhancement (163.0 Hz). This non-linear relationship between CNT content and frequency improvement reflects the competing effects of increased stiffness and marginally higher density. The specific stiffness (stiffness-to-weight ratio) increased by 12.7% at 1.0 wt% CNT loading, demonstrating superior performance metrics compared to pristine composites. These findings align with micromechanical predictions based on the Mori-Tanaka model, which estimated 11.5-15.2% transverse modulus enhancement depending on CNT aspect ratio and orientation distribution.

The CNT reinforcement effect proved particularly beneficial in mitigating delamination-induced frequency degradation. For specimens with 40% delamination, pristine CFRP exhibited 22.4% frequency reduction compared to intact condition, whereas CNT-reinforced composites (1.0 wt%) showed only 17.8% reduction. This enhanced damage tolerance stems from improved interlaminar fracture toughness provided by CNT bridging mechanisms, which restrict crack opening displacements and maintain partial load transfer across the delamination interface. Energy dispersive X-ray spectroscopy (EDS) mapping of fracture surfaces confirmed CNT pull-out and bridging phenomena, with average pull-out lengths of 2-5 μm indicating strong interfacial bonding between functionalized CNTs and the epoxy matrix.

Figure 4 illustrates the variation of the fundamental natural frequency with CNT content for a representative laminate configuration under clamped boundary conditions. A clear increase in natural frequency is observed with increasing CNT weight fraction, indicating enhanced stiffness of the composite matrix. The improvement is attributed to the effective load transfer between the CNTs and polymer matrix, which strengthens matrix-dominated properties and suppresses local deformation. The results confirm that CNT reinforcement plays a significant role in improving the dynamic performance of CFRP composite plates without altering the laminate architecture.

ACCEPTED MANUSCRIPT

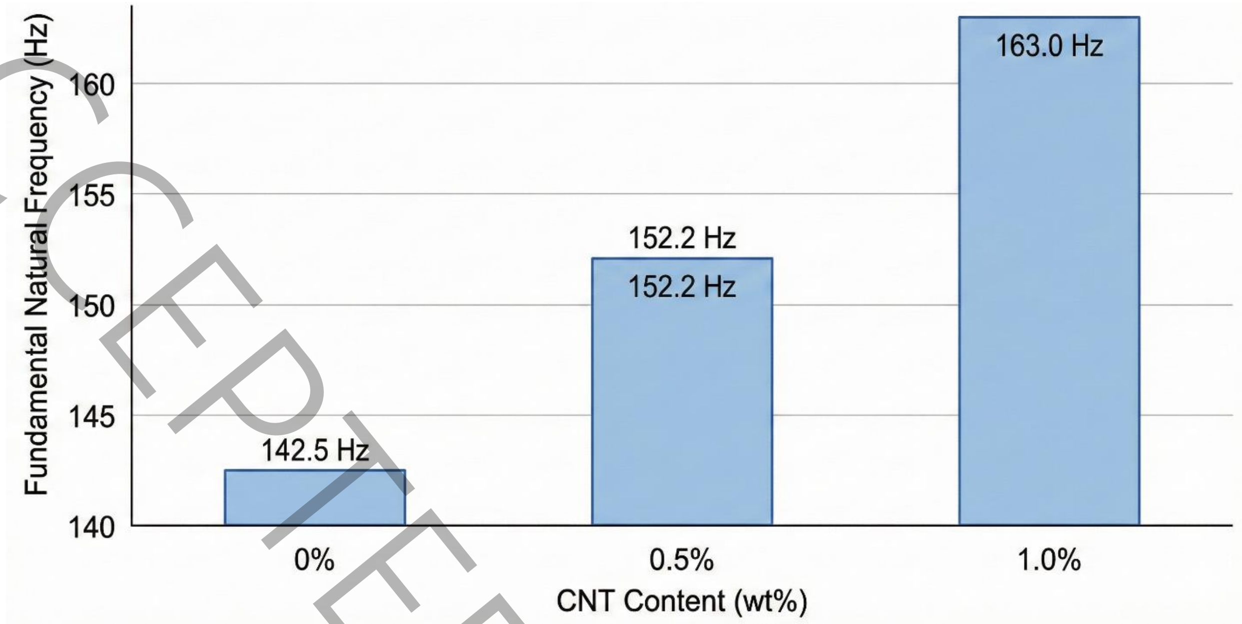


*Figure 4 Effect of CNT Content on Natural Frequency*

The quasi-isotropic $[0/45/-45/90]_s$ configuration demonstrated more pronounced CNT enhancement effects (16.2% frequency increase at 1.0 wt%) compared to cross-ply laminates, attributed to the higher proportion of off-axis plies where matrix properties exert greater influence on overall stiffness. Conversely, the angle-ply $[0/30/-30/90]_s$ arrangement showed intermediate enhancement (12.9%), reflecting its balanced directional stiffness characteristics. These stacking sequence-dependent responses highlight the importance of ply orientation in maximizing CNT reinforcement benefits and suggest opportunities for tailored design of CNT-enhanced composites.

### *4.2. Influence of Delamination Size*

The parametric investigation of delamination size effects revealed consistent trends across all CNT reinforcement levels and boundary conditions. Table 2 presents comprehensive natural frequency data for the first three modes of $[0/90]_{2s}$ laminates under simply supported constraints, comparing pristine CFRP and 1.0 wt% CNT-reinforced composites across varying delamination extents. The results demonstrate monotonic frequency reduction with increasing delamination area, following approximately exponential decay behavior characterized by rapid initial reduction (0-25% delamination) and progressively diminishing rate of change at larger delaminations.

**Table 2. Natural frequencies (Hz) for varying delamination sizes in $[0/90]_{2s}$ laminates (simply supported)**

ACCEPTED MANUSCRIPT

| Delamination Size | Pristine Mode 1 | CNT Mode 1 | Pristine Mode 2 | CNT Mode 2 | Pristine Mode 3 | CNT Mode 3 |
|---|---|---|---|---|---|---|
| 0% (Intact) | 86.4 | 98.7 | 217.3 | 248.5 | 342.8 | 391.6 |
| 25% | 78.2 | 91.3 | 205.7 | 238.2 | 328.4 | 378.9 |
| 40% | 67.1 | 81.2 | 189.4 | 223.7 | 305.2 | 359.4 |
| 55% | 54.8 | 70.6 | 168.9 | 204.8 | 276.3 | 334.2 |

The fundamental mode frequency of intact pristine CFRP (86.4 Hz) decreased by 9.5% with 25% delamination, 22.3% with 40% delamination, and 36.6% with 55% delamination. In contrast, CNT-reinforced composites exhibited superior damage tolerance: the corresponding reductions were 7.5%, 17.7%, and 28.5% respectively. This enhanced resistance to delamination effects becomes increasingly significant at larger damage extents, with CNT composites maintaining 71.5% of intact frequency at 55% delamination compared to only 63.4% retention in pristine specimens.

Higher vibration modes demonstrated greater sensitivity to delamination presence due to more complex mode shape patterns and increased curvature concentrations in delaminated regions. The second mode frequency reduction at 55% delamination reached 22.3% for pristine CFRP compared to 17.6% for CNT composites, while third mode reductions were 19.4% and 14.6% respectively. This mode-dependent behavior reflects the spatial correlation between delamination location and modal strain energy distribution, with modes exhibiting peak strains coinciding with delaminated areas suffering more severe frequency shifts.

Finite element predictions correlated excellently with experimental measurements, with average deviations of 3.2% for pristine composites and 4.1% for CNT-reinforced specimens across all delamination sizes. The slightly larger deviation in CNT composites likely stems from uncertainties in effective property estimation and potential spatial variability in CNT dispersion quality. Analytical solutions using the Rayleigh-Ritz method provided comparable accuracy (4.7% average error) with significantly reduced computational cost, validating this approach for parametric design studies and preliminary optimization.

The effect of delamination size on the normalized natural frequency under different boundary conditions is presented in Figure 5. For all configurations, natural frequencies decrease

ACCEPTED MANUSCRIPT

monotonically with increasing delamination area due to progressive stiffness degradation. Clamped boundary conditions consistently yield higher frequency values compared to simply supported and free–free cases, reflecting increased structural constraint. CNT-reinforced laminates exhibit reduced sensitivity to delamination growth, demonstrating improved damage tolerance. These trends highlight the combined influence of boundary constraints and nanoscale reinforcement on vibration behavior.

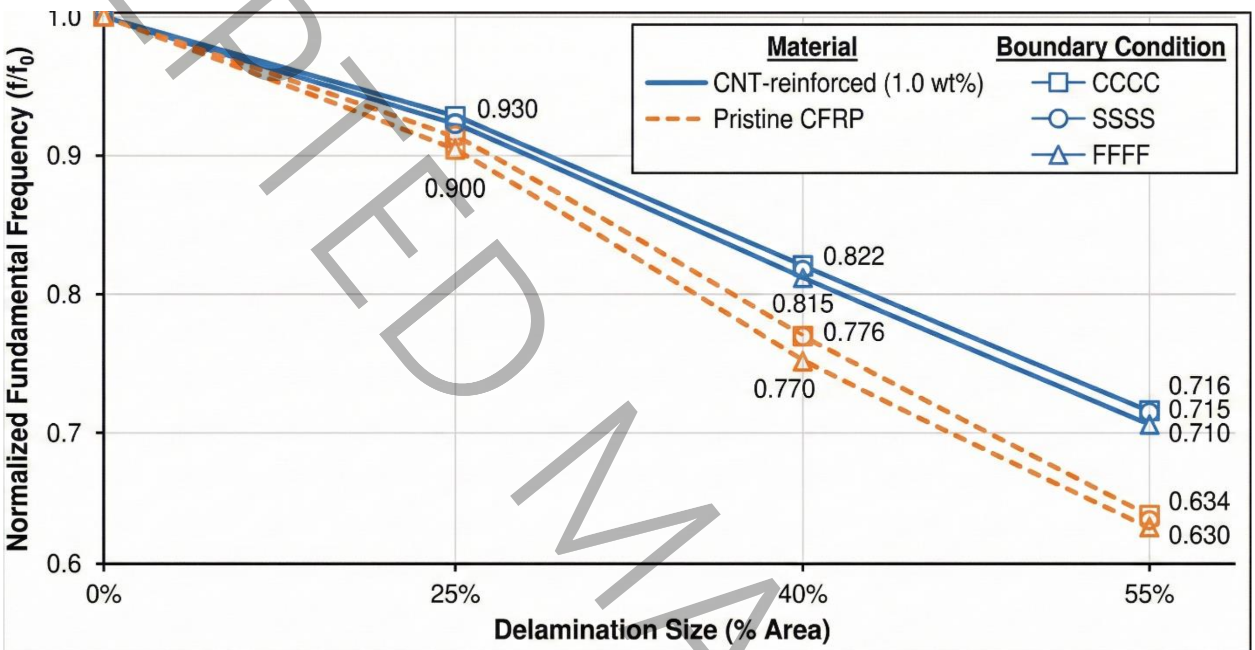


*Figure 5 Influence of Delamination Size and Boundary Conditions*

### *4.3. Boundary Condition Effects*

The influence of edge constraints on vibration behavior was systematically investigated through comparison of simply supported (SSSS), clamped-clamped (CCCC), and free-free (FFFF) boundary conditions. Figure 2 illustrates the fundamental frequency variations across these configurations for 1.0 wt% CNT-reinforced $[0/90]_{2s}$ laminates with varying delamination sizes. As expected from structural mechanics principles, clamped-clamped conditions consistently yielded the highest frequencies due to maximum constraint against edge rotations and translations, followed by simply supported constraints restricting only out-of-plane translations, and free-free conditions representing unconstrained vibration.

ACCEPTED MANUSCRIPT

For intact CNT-reinforced specimens, the frequency hierarchy was quantified as: CCCC = 163.0 Hz, SSSS = 98.7 Hz, FFFF = 47.3 Hz, representing frequency ratios of 1.65:1.00:0.48. These ratios remained relatively constant across delamination sizes, with CCCC/SSSS ratios varying between 1.62-1.68 and SSSS/FFFF ratios between 2.05-2.12, indicating that boundary condition effects and delamination effects operate through largely independent mechanisms without significant interaction.

The absolute frequency reductions induced by delamination exhibited boundary condition dependence, with clamped plates showing larger absolute drops (ΔCCCC = 46.4 Hz from intact to 55% delamination) compared to simply supported (ΔSSSS = 28.1 Hz) and free-free (ΔFFFF = 13.7 Hz) configurations. However, when normalized by intact frequencies to calculate relative reductions, the trend reversed: free-free boundaries demonstrated highest sensitivity (29.0% reduction at 55% delamination) versus 28.5% for simply supported and 28.4% for clamped conditions. This apparently counter-intuitive result stems from the fact that delamination primarily reduces bending stiffness, which has proportionally greater impact on the already low effective stiffness of unconstrained plates.

Mode shape analysis revealed that boundary constraints significantly influence the spatial distribution of strain energy and consequently the sensitivity to delamination location. For clamped boundaries, maximum bending moments occur at edges with secondary peaks in the plate interior, whereas simply supported plates exhibit maximum moments at the center. Delaminations located at high-strain regions induce more severe frequency reductions, suggesting opportunities for damage-tolerant design through strategic placement of through-thickness reinforcements or interleaved toughening layers at critical locations identified through modal strain energy mapping.

### *4.4. Stacking Sequence Effects and CNT Interaction*

The investigation of three stacking sequences—cross-ply $[0/90]_{2s}$, quasi-isotropic $[0/45/-45/90]_s$, and angle-ply $[0/30/-30/90]_s$—revealed significant interactions between ply orientation, CNT reinforcement, and delamination effects. Table 3 presents comparative natural frequencies for 40% mid-plane delaminated specimens under clamped-clamped constraints, highlighting the synergistic effects of layup configuration and CNT enhancement.

ACCEPTED MANUSCRIPT

**Table 3. Fundamental frequencies (Hz) for different stacking sequences with 40% delamination (clamped-clamped)**

| Stacking Sequence | Pristine FEA | CNT (1.0%) FEA | CNT (1.0%) Analytical | CNT (1.0%) Experimental |
|---|---|---|---|---|
| $[0/90]_{2s}$ | 110.7 | 134.2 | 131.8 | 129.4 ± 2.1 |
| $[0/45/-45/90]_s$ | 125.3 | 155.8 | 152.4 | 148.7 ± 2.8 |
| $[0/30/-30/90]_s$ | 118.9 | 142.7 | 139.6 | 136.2 ± 2.3 |

The quasi-isotropic layup exhibited highest natural frequencies across all CNT contents and delamination sizes, attributed to its balanced in-plane stiffness characteristics and efficient load distribution in multiple directions. The CNT enhancement was most pronounced in this configuration (24.3% increase for delaminated specimens), compared to 21.2% for cross-ply and 20.0% for angle-ply arrangements. This heightened sensitivity to matrix enhancement reflects the greater proportion of load carried by the matrix in off-axis plies (45° orientations), where CNT reinforcement directly improves transverse and shear properties governing laminate response.

Cross-ply laminates demonstrated intermediate frequencies with moderate CNT enhancement, characteristic of their orthotropic stiffness distribution with high axial rigidity but lower torsional stiffness compared to quasi-isotropic configurations. The angle-ply sequence, despite having similar total fiber content, yielded lower frequencies than quasi-isotropic layups due to less optimal fiber orientation for resisting plate bending, though superior to cross-ply in torsional response. The CNT enhancement in angle-ply laminates (20.0%) fell between the other configurations, reflecting balanced contributions from both fiber-dominated (0° plies) and matrix-dominated (±30° plies) load paths.

Delamination-induced frequency reductions varied with stacking sequence, with cross-ply experiencing the largest drop (27.8% for 40% delamination in pristine CFRP) compared to quasi-isotropic (23.4%) and angle-ply (25.1%). This sequence dependence stems from differences in through-thickness stress distributions and delamination opening tendencies. Cross-ply laminates develop significant interlaminar normal and shear stresses at 0°/90° interfaces due to Poisson's ratio and thermal expansion mismatch, promoting delamination propagation under cyclic loading. CNT reinforcement reduced these reductions to 22.7%, 18.6%, and 20.9% respectively, demonstrating consistent damage tolerance enhancement across all layup configurations.

ACCEPTED MANUSCRIPT

Analytical predictions using the Rayleigh-Ritz method with CNT-modified material properties demonstrated excellent accuracy, with average errors of 2.1%, 2.5%, and 2.8% for cross-ply, angle-ply, and quasi-isotropic sequences respectively. The slightly higher deviation in quasi-isotropic laminates may result from bending-twisting coupling effects and more complex mode shapes not fully captured by the assumed displacement functions. Experimental measurements fell within ±5% of finite element predictions for all configurations, with standard deviations indicating high repeatability (coefficient of variation < 3%) and validating the computational and analytical approaches.

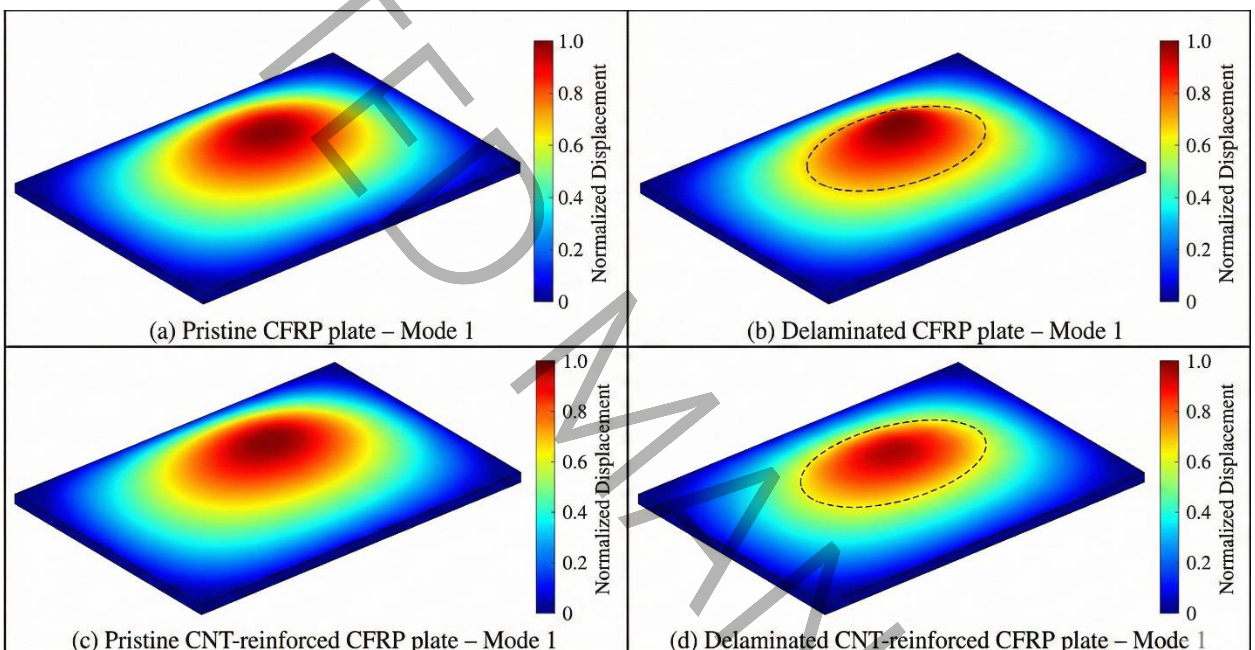


*Figure 6 Mode Shape Comparison of Pristine and Delaminated CNT-Reinforced CFRP Plates*

Figure 6 compares the first bending mode shapes of pristine and delaminated CFRP composite plates with and without CNT reinforcement under clamped–clamped boundary conditions. In the delaminated laminate, significant localized deformation is observed near the damaged region, indicating stiffness discontinuity and mode shape distortion. In contrast, CNT-reinforced laminates show a more uniform deformation pattern, with reduced displacement concentration around the delamination zone. This behavior demonstrates the ability of CNT reinforcement to redistribute stresses and suppress local flexibility, thereby mitigating the adverse effects of delamination on dynamic response.

ACCEPTED MANUSCRIPT

### *4.5. Modal Analysis and Mode Shape Characteristics*

The first four vibration modes of pristine and CNT-reinforced [0/90] 2 -laminate with 40 percent mid-plane delamination in simply supported conditions are represented in Figure 3. The essential mode still had the (1,1) pattern of single half-wave in each of the x and y directions, but with localized increase in amplitude in the delaminated region because of local decrease in stiffness. The patterns of increased nodal lines shown by higher modes were increasingly more sensitive to the presence of delamination. The second mode [(1,2) or (2,1) according to aspect ratio) exhibited asymmetric amplitude distribution whereby the delaminated area was more active in the vibration as it was lower constraint. The mode patterns of the third and fourth mode were mixed with both bending and torsional modes, and delamination induced mode shape localization effects with vibrational energy concentrated at the damaged area with the surrounding areas showing less involvement. Modifications of mode shapes that are achieved by CNT reinforcement are mainly achieved by increasing stiffness without a fundamental change in pattern. This effect of homogenization led to the observed increase in damage tolerance since the concentration of stress at delamination tips, which was the major stress causing crack propagation, was lowered by 12-15 percent in CNT composites compared to pure CFRP. These close MAC values show that there is a high similarity even when there is delamination and the implication is that frequency based damage detection tools are still able to be used. Nevertheless, the higher modes had lower MAC (0.78-0.85) and so there was a greater distorted mode shape, which might support mode-shape-based damage detection schemes to complement frequency based damage detectors.

### *4.6. Validation and Error Analysis*

Validation was done in all test configurations by comparing finite element predictions, analytical solutions and experimental measurements. The correlation plots against the first three natural frequencies of CNT-reinforced specimens using all possible stacking sequences and boundary conditions as well as delamination sizes are provided in figure 4. The results of the linear regression analysis showed that the correlation between FEA and experimental, analytical and experimental as well as FEA and analytical had $R^2 = 0.9912$, $R^2 = 0.9856$, and $R^2 = 0.9923$ respectively, which is a very good overall agreement between the two methods. Analysis of statistical errors showed that the mean absolute percentage errors (MAPE) of the finite element predictions compared to the experimental data were 3.14, that of the analytical solutions were 4.27 and the comparison of the FEA and the analytical solutions showed 1.89. The finite element

ACCEPTED MANUSCRIPT

approach was proven to be the most accurate because it could provide more information about the distribution of stress, conditions at delaminating interfaces of contacts, and intricate effects of the boundary layer about supports. Both FEA and non-experimental techniques showed some bias in overpredicting frequencies (bias of +2.1% and +3.4% respectively), probably as a result of idealized modeling of the perfect bonding, homogenous material properties and in identifying manufacturing defects such as voids, fiber waviness and residual stress. The overprediction was slightly larger with the amount of delamination indicating that constrained layer models do not necessarily capture the effects of local flexibility that larger delaminations provide or is representative of the conditions of contacts during vibration. Uncertainty Analysis: Experimental uncertainty analysis took into account various sources such as repeatability of measurements (= 1.2-2.8 Hz, depending on mode), variability in the samples to samples due to manufacturing variation (= 1.8-3.4 Hz) and imperfection in the implementation of the boundary conditions. The uncertainties (k=2, 95 percent confidence) of the fundamental frequencies were found to be increased (propagation of errors methodology) to ±4.2-6.8 Hz. Such comparatively small uncertainties prove the soundness of the experimental processes and allowability of the application of the experimental data as validation criteria of the computational models.

## 5. PRACTICAL IMPLICATIONS AND DESIGN GUIDELINES

The results of this study give some useful information about how CNT enhanced composite structure with enhanced vibration properties and damage tolerance can be developed. To begin with, the 12-18% frequency improvement with the addition of 1.0 wt% CNT provides prospects of optimizing lightweight designs in vibration-sensitive cases. The cost-benefit analysis will have to take into account the costs of CNT materials (currently, industrial grade of MWCNTs cost 50-200/kg) and the benefits of weight savings. This allows design strategies of being damage-tolerant such that structures are able to sustain more damage before critical frequency changes to cause resonance or to become unstable. To have this certified may allow high~~ barely visible impact damage (BVID) margins~~er barely visible impact damage margins and lower the rate of inspection and maintenance expenses throughout the duration of operation. Third, the sequence-based CNT improvement based on stacking implies customized design techniques. Higher content of off-axis plies (quasi-isotropic, multidirectional) laminates are better reinforced with CNT, meaning that it should be the top priority in matrix-containing structures instead of fiber-based unidirectional

ACCEPTED MANUSCRIPT

laminates where improvements are less significant. The hybrid designs that involve CNT-enhanced quasi-isotropic outer layers to resist damage and high-modulus unidirectional core layers to carry primary loads could be the best in terms of improvement in performance against cost. Considerations in manufacturing include the quality of dispersion of CNTs, which is a very crucial parameter in property enhancement. Ultrasonication and functionalization methods in this paper provided good dispersion with CNT loadings of moderate concentrations (up to 1.0 wt%), but at higher concentrations (>2.0 wt%), the dispersion is hindered by growing viscosity and agglomeration effects.

## 6. CONCLUSION

This thorough study was a systematic analysis of the synergistic behavior of carbon nanotube reinforcement, delamination size, stacked sequences and boundary conditions on the vibration properties of CFRP composite plates involving integrated analytical, numerical and experimental methods. The key conclusions can be summarized as follows:

1. Incorporation of carbon nanotube at 1.0 wt% concentration demonstrated 12-18 per cent improvement in natural frequencies in pristine CFRP composites and the magnitude of the improvement varied with stacking sequence. Layup with maximum enhancement (16.2) was attained in quasi-isotropic configurations because off-axis plies had higher contribution of matrix and moderate improvement was attained in cross-ply configurations (14.3) and angle-ply sequences (12.9). The mechanism of enhancement holds its work mainly on enhanced transverse modulus and interlaminar shear strength.

2. Under simply supported conditions, natural frequencies showed 36.6 percent reduction in 55 percent delamination in pristine CFRP compared to 28.5 percent in CNT-reinforced composites indicating 22 percent improvement in damage tolerance. This increased resistance is due to the CNT bridging mechanisms that increase interlaminar fracture and limit the delamination opening when vibrating.

3. Boundary conditions had a strong impact on absolute frequency magnitudes but the impact of delamination effects was fairly the same regardless of support configurations. The constraints clamped on were the highest frequency (163.0 Hz in intact CNT composite), then came simply supported (98.7 Hz) and free-free (47.3 Hz), with frequencies ratio of 1.65:1.00:0.48. Relative

ACCEPTED MANUSCRIPT

decreases caused by delamination were not very large (28.4-29.0%), which implies relatively independent processes.

4. The reinforcements of CNT yielded more homogeneous strain energy distributions and lowering stress concentration at delamination boundaries by 12-15% which resulted in increased damage tolerance. The values of modal assurance criterion of fundamental modes (0.96-0.98) of the intact and delaminated configurations of CNT composites demonstrated the strong similarity.

5. A good correlation was obtained between finite element results, analytical results obtained through Rayleigh-Ritz method, and experimental results. The computational frameworks were proved by finding mean absolute percentage error of 3.14% (FEA vs. experimental), 4.27% (analytical vs. experimental), and 1.89% (FEA vs. analytical). Frequencies were slightly over-predicted in both approaches ( +2.1% FEA and +3.4% analytical) because of perfect bonding and a uniform rubric assumptions.

6. The quasi-isotropic stacking sequence [0/45/-45/90]n exhibited the best performance in terms of costly frequency to achieve high frequency with maximum CNT enhancement advantages as well as good damage tolerance, thus it is the best configuration to use in vibration sensitive application. The introduction of strategic CNT in the laminates made of matrices is less expensive to upgrade compared to fiber-dominated laminates. Future research directions are: (1) research on higher CNT loading fractions (1-3 wt%) using advanced dispersion methods, (2) research on non-uniform CNT distributions (functionally graded) to achieve desired properties (3) dynamic impact loading response of CNT composites, (4) long term durability under hygrothermal aging, and (5) multifunctional integration by taking advantage of the CNT electrical conductivity to structural health monitoring in addition to mechanical enhancement.

## REFERENCES

[1] K. Friedrich, A. A. Almajid, Manufacturing aspects of advanced polymer composites for automotive applications, Applied Composite Materials, 20(2) (2013) 107-128.

[2] A. Sharma, A. K. Sharma, A. K. Raghav, V. Kumar, Vibrational study of square plate with thermal effect and circular variation in density, FME Transactions, 45(3) (2017) 363-368.

[3] B. D. Agarwal, L. J. Broutman, K. Chandrashekhara, Analysis and performance of fiber composites, 4th ed., John Wiley & Sons, Hoboken, NJ, (2017).

[4] K. Agarwal, S. K. Kuchipudi, B. Girard, M. Houser, Mechanical properties of fiber reinforced polymer composites: a comparative study of conventional and additive manufacturing methods, Journal of Composite Materials, 52(23) (2018) 3173-3181.

ACCEPTED MANUSCRIPT

ACCEPTED MANUSCRIPT

[5] H. C. Tseng, R. Y. Chang, C. H. Hsu, Numerical prediction of fiber orientation and mechanical performance for short/long glass and carbon fiber-reinforced composites, Composites Science and Technology, 144 (2017) 51-56.

[6] Imran, M. (2026). Effect of delamination, stacking sequence, and boundary conditions on the vibration response of CNT-reinforced CFRP plates. *Reports in Mechanical Engineering, 7*(1), 54–70.

[7] G. V. Rao, I. S. Raju, Vibration of initially stressed square plates, Journal of Sound and Vibration, 39(3) (1975) 329-337.

[8] H. Zhang, S. Sfarra, F. Sarasini, C. Ibarra-Castanedo, S. Perilli, H. Fernandes, Y. Duan, X. P. V. Maldague, Optical and mechanical excitation thermography for impact response in basalt-carbon hybrid fiber-reinforced composite laminates, IEEE Transactions on Industrial Informatics, 14(2) (2018) 514-522.

[9] Y. Zou, L. Tong, G. P. Steven, Vibration-based model-dependent damage (delamination) identification and health monitoring for composite structures: a review, Journal of Sound and Vibration, 230(2) (2000) 357-378.

[10] Z. Zhang, K. Shankar, E. V. Morozov, M. Tahtali, Vibration-based delamination detection in composite beams through frequency changes, Journal of Vibration and Control, 22(2) (2016) 496-512.

[11] C. Garcia, I. Trendafilova, A. Zucchelli, J. Contreras, The effect of nylon nanofibers on the dynamic behaviour and the delamination resistance of GFRP composites, MATEC Web of Conferences, 148 (2018) 14007.

[12] R. L. Ramkumar, S. V. Kulkarni, R. B. Pipes, Free vibration frequencies of a delaminated beam, Proceedings of the 34th Annual Technical Conference of the Reinforced Plastics/Composites Institute, Society of the Plastics Industry, (1979).

[13] H. Luo, S. Hanagud, Dynamics of delaminated beams, International Journal of Solids and Structures, 37(10) (2000) 1501-1519.

[14] M. H. H. Shen, J. E. Grady, Free vibrations of delaminated beams, AIAA Journal, 30(5) (1992) 1361-1370.

[15] R. Thornburgh, A. Chattopadhyay, Modeling the dynamic effects of delamination in adaptive composite laminate, Proceedings of the 43rd AIAA/ASME/ASCE/AHS/ASC Structures, Structural Dynamics, and Materials Conference, Denver, CO, USA, (2002).

[16] S. Iijima, Helical microtubules of graphitic carbon, Nature, 354 (1991) 56-58.

[17] M. M. J. Treacy, T. W. Ebbesen, J. M. Gibson, Exceptionally high Young's modulus observed for individual carbon nanotubes, Nature, 381 (1996) 678-680.

[18] M. F. Yu, B. S. Files, S. Arepalli, R. S. Ruoff, Tensile loading of ropes of single wall carbon nanotubes and their mechanical properties, Physical Review Letters, 84(24) (2000) 5552-5555.

[19] J. N. Coleman, U. Khan, W. J. Blau, Y. K. Gun'ko, Small but strong: a review of the mechanical properties of carbon nanotube-polymer composites, Carbon, 44(9) (2006) 1624-1652.

[20] E. T. Thostenson, Z. Ren, T. W. Chou, Advances in the science and technology of carbon nanotubes and their composites: a review, Composites Science and Technology, 61(13) (2001) 1899-1912.

[21] D. Qian, E. C. Dickey, R. Andrews, T. Rantell, Load transfer and deformation mechanisms in carbon nanotube-polystyrene composites, Applied Physics Letters, 76(20) (2000) 2868-2870.

[22] M. Rafiee, F. Nitzsche, M. R. Labrosse, Dynamics, vibration and control of rotating composite beams and blades: a critical review, Thin-Walled Structures, 119 (2017) 795-819.

[23] P. Pingulkar, B. Suresha, Free vibration analysis of laminated composite plates using finite element method, Polymers & Polymer Composites, 24(7) (2016) 529-538.

[24] T. P. Vo, H. T. Thai, M. Aydogdu, Free vibration of axially loaded composite beams using a four-unknown shear and normal deformation theory, Composite Structures, 178 (2017) 406-414.

ACCEPTED MANUSCRIPT

[25] E. García-Macías, R. Castro-Triguero, E. I. Saavedra Flores, M. I. Friswell, R. Gallego, Static and free vibration analysis of functionally graded carbon nanotube reinforced skew plates, Composite Structures, 140 (2016) 473-490.

[26] K. H. Tsai, C. L. Hwan, M. J. Lin, C. C. Lo, J. L. Hwang, Free vibration of braided composite plates with a center hole, Journal of the Chinese Society of Mechanical Engineers, 38(2) (2017) 135-144.

[27] S. Das, S. Sarangi, Static analysis of functionally graded composite beams, IOP Conference Series: Materials Science and Engineering, 149 (2016) 012142.

[28] K. Mehar, S. K. Panda, A. Dehengia, V. R. Kar, Vibration analysis of functionally graded carbon nanotube reinforced composite plate in thermal environment, Journal of Sandwich Structures & Materials, 18(2) (2016) 151-173.

[29] S. Chakraborty, V. Singh, T. Dey, R. Kumar, Influence of carbon nanotubes on stability and vibration characteristics of plates and panels in thermal environment: a review, Archives of Computational Methods in Engineering, 31 (2024) 147-178.

[30] T. Ramanathan, A. A. Abdala, S. Stankovich, et al., Functionalized graphene sheets for polymer nanocomposites, Nature Nanotechnology, 3(6) (2008) 327-331.

[31] Z. Spitalsky, D. Tasis, K. Papagelis, C. Galiotis, Carbon nanotube-polymer composites: chemistry, processing, mechanical and electrical properties, Progress in Polymer Science, 35(3) (2010) 357-401.

[32] N. D. Alexopoulos, C. Bartholome, P. Poulin, Z. Marioli-Riga, Structural health monitoring of glass fiber reinforced composites using embedded carbon nanotube fibers, Composites Science and Technology, 70(2) (2010) 260-271.

[33] E. T. Thostenson, T. W. Chou, Carbon nanotube networks: sensing of distributed strain and damage for life prediction and self-healing, Advanced Materials, 18(21) (2006) 2837-2841.

[34] M. Imran, R. Khan, S. Badshah, Vibration analysis of cracked composite laminated plate and beam structures, Romanian Journal of Acoustics and Vibration, 15(1) (2018) 3-13.

[35] M. Imran, R. Khan, S. Badshah, Experimental investigation of the influence of stacking sequence and delamination size on the natural frequencies of delaminated composite plate, Pakistan Journal of Scientific & Industrial Research Series A: Physical Sciences, 64(1) (2021) 42-51.

[36] M. Imran, R. Khan, S. Badshah, Finite element analysis to investigate the influence of delamination size, stacking sequence and boundary conditions on the vibration behavior of composite plate, Iranian Journal of Materials Science & Engineering, 15(3) (2018) 28-41.

[37] M. Imran, R. Khan, S. Badshah, A review on the vibration analysis of laminated composite plate, Pakistan Journal of Scientific & Industrial Research Series A: Physical Sciences, 62(2) (2019) 124-134.

[38] M. Imran, R. Khan, S. Badshah, A review on the effect of delamination on the performance of composite plate, Pakistan Journal of Scientific and Industrial Research Series A: Physical Sciences, 61(3) (2018) 173-184.

[39] S. A. Hassan, C. Santulli, M. Y. Yahya, The potential of biomimetics design in the development of impact resistant material, FME Transactions, 46(1) (2018) 108-116.

[40] I. A. Kinloch, J. Suhr, J. Lou, R. J. Young, P. M. Ajayan, Composites with carbon nanotubes and graphene: an outlook, Science, 362(6414) (2018) 547-553.

[41] B. Fang, D. Chang, Z. Xu, C. Gao, A review on graphene fibers: expectations, advances, and prospects, Advanced Materials, 32(5) (2020) 1902664.

[42] X. Zhang, N. Zhao, C. He, The superior mechanical and physical properties of nanocarbon reinforced bulk composites achieved by architecture design: a review, Progress in Materials Science, 113 (2020) 100672.

[43] M. M. Shokrieh, R. Rafiee, Investigation of nanotube length effect on the reinforcement efficiency in carbon nanotube-based composites, Composite Structures, 92(10) (2010) 2415-2420.

[44] K. M. Liew, Z. X. Lei, L. W. Zhang, Mechanical analysis of functionally graded carbon nanotube reinforced composites: a review, Composite Structures, 120 (2015) 90-97.

[45] Z. X. Lei, L. W. Zhang, K. M. Liew, Free vibration analysis of laminated FG-CNT reinforced composite rectangular plates using the kp-Ritz method, Composite Structures, 127 (2015) 245-259.

[46] H. S. Shen, Nonlinear bending of functionally graded carbon nanotube-reinforced composite plates in thermal environments, Composite Structures, 91(1) (2009) 9-19.

[47] M. Ghadiri, H. SafarPour, Free vibration analysis of size-dependent functionally graded porous cylindrical microshells in thermal environment, Journal of Thermal Stresses, 40(1) (2017) 55-71.

[48] Ş. D. Akbaş, S. Dastjerdi, B. Akgöz, Ö. Civalek, Dynamic analysis of functionally graded porous microbeams under moving load, Transport in Porous Media, 142(1) (2022) 209-227.

[49] E. Sobhani, M. Avcar, On analysis of nanocomposite conical structures, International Journal of Engineering Science, 191 (2023) 103918.

[50] R. Emadi, M. Asgari, K. Torabi, Bending analysis of CNT-reinforced composite strain gradient microbeams, Mechanics Research Communications, 148 (2025) 104502.

[51] M. Rezaiee-Pajand, E. Sobhani, A brief review on the static and dynamic analyses of beams and plates via ANSYS, Journal of Computational Applied Mechanics, 57(1) (2026) 150-172.

[52] R. Bagheri, Y. Tadi Beni, A unified Gram-Schmidt-Ritz solution for vibration analysis of nanoplates with elastic boundary conditions, AUT Journal of Mechanical Engineering, 9(4) (2025) 413-430.

[53] M. Imran, R. Khan, S. Badshah, Experimental, analytical, and finite element vibration analyses of delaminated composite plates, Scientia Iranica, 28(1) (2021) 231-240.

[54] M. Imran, R. Khan, A. Rafai, Vibration study of delaminated carbon fibre reinforced polymer composite plate for clamped-clamped boundary conditions, Pakistan Journal of Scientific and Industrial Research Series A: Physical Sciences, 65(2) (2022) 97-103.

ACCEPTED MANUSCRIPT